# Inelastic X-Ray Scattering in Correlated Mott Insulators

T. P. Devereaux and G. E. D. McCormack
*Department of Physics, University of Waterloo, Waterloo, Ontario, Canada*

J. K. Freericks
*Department of Physics, Georgetown University, Washington, D.C.*
(Received 2 August 2002; published 14 February 2003)

We calculate the inelastic light scattering from x rays, which allows the photon to transfer both energy and momentum to the strongly correlated charge excitations. We find that the charge-transfer peak and the low-energy peak both broaden and disperse through the Brillouin zone similar to what is seen in experiments in materials such as $Ca_2CuO_2Cl_2$.

DOI: 10.1103/PhysRevLett.90.067402 PACS numbers: 78.70.Ck, 71.30.+h, 72.80.Sk, 78.66.Nk

The dynamics of electrons in strongly correlated systems is far from well understood. In a Mott insulator, correlations split a single band into a lower and an upper Hubbard band separated by a Mott gap. Many experimental probes have focused attention on exploring the detailed nature of the lower Hubbard band from which electrons may be excited using angle-resolved photoemission, for example, but the structure and symmetry of the upper Hubbard band and the relaxational dynamics of electrons populated into it remains largely unexplored.

Inelastic x-ray scattering [1] has attempted to address this issue on a number of correlated insulators such as $La_2CuO_4$ and $Sr_2CuO_2Cl_2$ [2], $Ca_2CuO_2Cl_2$ [3], $NaV_2O_5$ [4], $Nd_2CuO_4$ [5], and 1D insulators $Sr_2CuO_2Cl_2$ and $Sr_2CuO_2$ [6]. The measured signal is resonantly enhanced by tuning the incident photon energy to lie near the Cu $K$ or V $L_3$ edge. The measurements have revealed remarkably similar characteristics as a function of photon energy loss: (i) the presence of a large, sharp, and relatively dispersionless peak centered around a few eVs, and (ii) the development of a low-energy peak dispersive towards higher frequencies for photon momentum transfers from the Brillouin zone (BZ) center along either the BZ edge or diagonal. Data taken on $Ca_2CuO_2Cl_2$ [3] are shown in Fig. 1. The high-energy peak has been associated with photon-induced charge transfer between orbitals of different atoms [4] or different orbitals of the same atom [3,6], while the low-frequency peak has been associated with a transition from the lower to upper Hubbard band across an effective Mott gap [3,4,6] and a $q$ dependence of the Mott gap has been inferred [2]. However, it does not seem obvious why an excitation across a Mott gap would show dispersion given that the physics of the Mott transition is local in character.

Theoretical calculations on inelastic x-ray scattering have been limited to energy-band model calculations and exact diagonalization studies of small clusters [1]. While energy-band calculations might be appropriate for ground-state properties of weakly correlated systems they do not adequately address the role of intra-atomic electron correlations which crucially affect properties of the charge excitation spectra of strongly correlated systems. Exact diagonalization studies of small clusters [3,7] largely focus on the energy separation between the states excitable by the x rays (such as excitons), and suffer the limitation that the line shape of the calculated spectra depend sensitively on cluster size due to finite size effects on the electron dynamics. Thus we need to formulate a theory for inelastic x-ray scattering which does not suffer from size effects and is able to account for atomic electron correlations.

Two important features of the experimental data have yet to be clarified. First, the selection rules coming from the different orientations of the *polarization* directions of the incoming and outgoing photons as well as the direction of their scattered momenta have not been used to determine the *symmetry* of the upper Hubbard band, for example. These selection rules have led to intense investigation of the dynamics of electrons in the high-temperature superconductors to determine information about charge dynamics on regions of the BZ or the

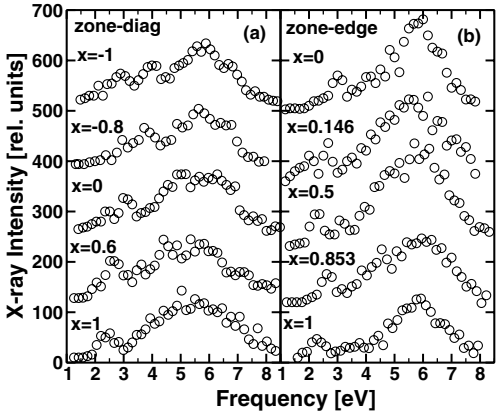


FIG. 1. Experimental data for $Ca_2CuO_2Cl_2$ [3] with momentum transfers along the BZ diagonal (a) and BZ edge (b), respectively. The values of the parameter $X = [\cos(q_x a) + \cos(q_y a)]/2$ indicate the values of the momentum transfer $(q_x, q_y)$. Note that for panel (b) the momentum transfer runs from $(0, 0)$ to $(\pi, 0)$ only, $X = 1$ to 0.

  

symmetry of the order parameter in the superconducting state [8]. Second, the mechanisms of electronic relaxation revealed by inelastic x-ray scattering have yet to be explored. More precisely, besides the magnitude of the matrix elements coupling the conduction band to the excited states via the photon vector potential, the way in which the x-ray induced charge imbalance relaxes, has remained largely unexplored. Inelastic x-ray scattering provides a window to investigate the symmetry and pathway of charge dynamics in strongly correlated systems.

We choose to focus attention on nonresonant x-ray scattering, or scattering in which the frequency dependence of the incoming or outgoing photons can be individually neglected and only the frequency shift $\Omega = \omega_i - \omega_s$ enters, where $\omega_{i,s}$ denotes incident, scattered x-ray energies, respectively. This means that we have lost the ability to make quantitative predictions concerning the overall intensity of the scattering and we cannot calculate line-shape changes induced by varying the incident photon frequency. However, our goal is to evaluate inelastic x-ray scattering in a model in which the correlations can be handled exactly — the Falicov-Kimball model in infinite dimensions — to determine which features emerge from the strong correlations. We note that our prior exact results for Raman scattering in both the Falicov-Kimball [9] and the more realistic Hubbard model [10] yield the same qualitative behavior in the insulating phases, so we expect inelastic x-ray scattering to also be model independent.

The Falicov-Kimball model, which has been used to describe a variety of phenomena in binary alloys [11], contains itinerant band electrons and localized electrons, in which the band electrons can hop with amplitude $t^*/2\sqrt{d}$ between nearest neighbors and interact via a screened Coulomb interaction $U$ with the localized electrons:

$$H = -\frac{t^*}{2\sqrt{d}}\sum_{\langle i,j\rangle} c_i^\dagger c_j + E_f \sum_i w_i - \mu \sum_i c_i^\dagger c_i + U \sum_i c_i^\dagger c_i w_i, \tag{1}$$

where $c_i^\dagger, c_i$ is the spinless conduction electron creation (annihilation) operator at site $i$ and $w_i = 0$ or 1 is a classical variable of the localized electron number at site $i$. $E_F$ and $\mu$ control the filling of the localized and conduction electrons, respectively.

In this single-band model with energy $\epsilon(\mathbf{k})$, the inelastic x-ray response is given formally by a density-density correlation function $S(\mathbf{q}, \omega) = -\frac{1}{\pi}[1 + n(\omega)]\chi''(\mathbf{q}, \omega)$ with

$$\chi(\mathbf{q}, \omega) = \langle [\tilde{\rho}(\mathbf{q}), \tilde{\rho}(-\mathbf{q})] \rangle_{(\omega)} \tag{2}$$

formed with an "effective" density operator given by

$$\tilde{\rho}(\mathbf{q}) = \sum_{\mathbf{k},\sigma} \gamma_a(\mathbf{k}) c_\sigma^\dagger(\mathbf{k} + \mathbf{q}/2) c_\sigma(\mathbf{k} - \mathbf{q}/2). \tag{3}$$

The strength of the scattering $\gamma_a$ is determined by the curvature of the band as

$$\gamma_a(\mathbf{k}) = \sum_{\alpha,\beta} e_\alpha^s \frac{\partial^2 \epsilon(\mathbf{k})}{\partial k_\alpha \partial k_\beta} e_\beta^i. \tag{4}$$

Here $\mathbf{e^{i,s}}$ denote the incident, scattered x-ray polarization vectors, respectively, and we have chosen units $k_B = c = \hbar = 1$ and have set the hypercubic lattice constant equal to 1. We can classify the scattering amplitudes by point group symmetry operations. If we choose $e^i = (1, 1, 1, ...)$ and $e^s = (1, -1, 1, -1, ...)$, then we have the $B_{1g}$ sector, while $e^i = e^s = (1, 1, 1, ...)$ projects out the $A_{1g}$ sector since the $B_{2g}$ component is identically zero in our model due to the inclusion of only nearest-neighbor hopping. We thus can cast the scattering amplitudes into a simple form: $\gamma_{A_{1g}}(\mathbf{k}) = -\epsilon(\mathbf{k})$ and $\gamma_{B_{1g}}(\mathbf{k}) = t^* \sum_{j=1}^{\infty} \cos \mathbf{k}_j (-1)^j/\sqrt{d}$.

The Dyson equation for the density-density correlation function appears in Fig. 2. Note that there are two coupled equations illustrated in Figs. 2(a) and 2(b); these equations differ by the number of $\gamma_a$ factors in them. The irreducible vertex function $\Gamma$ is the dynamical charge vertex [12] which takes the form

$$\Gamma(i\omega_m, i\omega_n; i\nu_{l\neq 0}) = \delta_{mn} \frac{1}{T} \frac{\Sigma_m - \Sigma_{m+l}}{G_m - G_{m+l}}, \tag{5}$$

on the imaginary axis [$i\omega_m = i\pi T(2m + 1)$ is the Fermionic Matsubara frequency and $i\nu_l = 2i\pi Tl$ is the Bosonic Matsubara frequency]. Here $\Sigma_m = \Sigma(i\omega_m)$ is the local self-energy on the imaginary axis and $G_m = G(i\omega_m)$ is the local Green's function on the imaginary axis. If the scattering amplitude $\gamma$ does not have a projection onto the full symmetry of the lattice, then there are no vertex corrections from the local dynamical charge vertex [13].

A straightforward calculation shows that the $B_{1g}$ response has no vertex corrections on the zone-diagonal

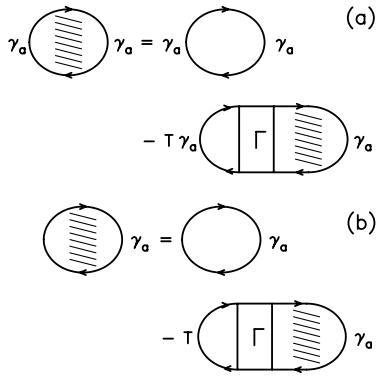


FIG. 2. Coupled Dyson equations for the inelastic x-ray scattering correlation functions described by the scattering amplitude $\gamma_a$. Panel (a) depicts the equation for the interacting correlation function, while panel (b) is the supplemental equation needed to solve for the correlation function. The symbol $\Gamma$ stands for the local dynamical irreducible charge vertex given in Eq. (5). In situations where there are no charge vertex corrections, the correlation function is simply given by the bare-bubble diagram in (a).

$\mathbf{q} = (q, q, q, q, \ldots)$. Hence, the $B_{1g}$ response is the bare bubble:

$$\chi_{B_{1g}}(\mathbf{q}, \nu) = \frac{i}{4\pi}\int_{-\infty}^{\infty} d\omega\{f(\omega)\chi_0(\omega; X, \nu) - f(\omega + \nu)\chi_0^*(\omega; X, \nu) - [f(\omega) - f(\omega + \nu)]\tilde{\chi}_0(\omega; X, \nu)\}, \tag{6}$$

with

$$\chi_0(\omega; X, \nu) = -\int_{-\infty}^{\infty} d\epsilon\rho(\epsilon)\frac{1}{\omega + \mu - \Sigma(\omega) - \epsilon}\frac{1}{\sqrt{1 - X^2}}F_\infty\left(\frac{\omega + \nu + \mu - \Sigma(\omega + \nu) - X\epsilon}{\sqrt{1 - X^2}}\right), \tag{7}$$

and

$$\tilde{\chi}_0(\omega; X, \nu) = -\int_{-\infty}^{\infty} d\epsilon\rho(\epsilon)\frac{1}{\omega + \mu - \Sigma^*(\omega) - \epsilon}\frac{1}{\sqrt{1 - X^2}}F_\infty\left(\frac{\omega + \nu + \mu - \Sigma(\omega + \nu) - X\epsilon}{\sqrt{1 - X^2}}\right). \tag{8}$$

Here we have used the following notation: $f(\omega) = 1/[1 + \exp(\omega)]$ is the Fermi-Dirac distribution, $\rho(\epsilon) = \exp(-\epsilon^2)/\sqrt{\pi}$ is the noninteracting density of states; $\Sigma(\omega)$ is the local self-energy on the real axis; $X = \lim_{d\to\infty}\sum_i \cos q_i/d$; and $F_\infty(z) = \int d\epsilon\rho(\epsilon)/(z - \epsilon)$ is the Hilbert transform of the noninteracting density of states. Techniques for finding the self-energy [14] have appeared elsewhere.

The $A_{1g}$ response everywhere and the $B_{1g}$ response off of the zone diagonal, do have vertex corrections. The calculation of each response function is straightforward, but tedious. One needs to first solve the coupled equations depicted in Fig. 2 on the imaginary axis and then perform the analytic continuation as in the Raman scattering case [9]. The end result is cumbersome and will be presented elsewhere.

The results for a correlated insulator $U = 4t^*$ at different temperatures are shown in Figs. 3 and 4 for $B_{1g}$ and $A_{1g}$ inelastic x-ray scattering, respectively, as a function of transferred energy for different momentum transfers throughout the BZ measured by the factor $X$. Panel (a) for Figs. 3 and 4 refers to scattering along the zone-diagonal $X = \cos q$ for the zone-diagonal wave vector $\mathbf{q} = (q, q, q, \ldots, q)$, and panel (b) refers to scattering along the zone edge [here we have $\mathbf{q} = (q, 0, q, 0, \ldots, q, 0)$ for $1 \geq X = (1 + \cos q)/2 \geq 0$ and $\mathbf{q} = (\pi, q, \pi, q, \ldots, \pi, q)$ for $0 \geq X = (-1 + \cos q)/2 \geq -1$. The curves have been shifted vertically for clarity. The lowest set of curves $X = 1$ corresponds to Raman scattering with optical photons [9]. The main qualitative feature in both figures is the presence of a small, dispersive low-energy peak for frequencies $\sim t^*$ and a large, dispersionless charge-transfer peak $\sim U$. While the charge-transfer peak remains relatively robust with increasing temperature, the low-energy peak gains intensity from zero as temperature is increased. In particular, all momenta show the development of low-energy spectral weight as $T$ increases and there is a nondispersive isosbestic point—a frequency at which the spectra are temperature independent—around $\nu \sim U/2$. The high-energy peak reflects the energy scale for excitations across the Mott gap and is

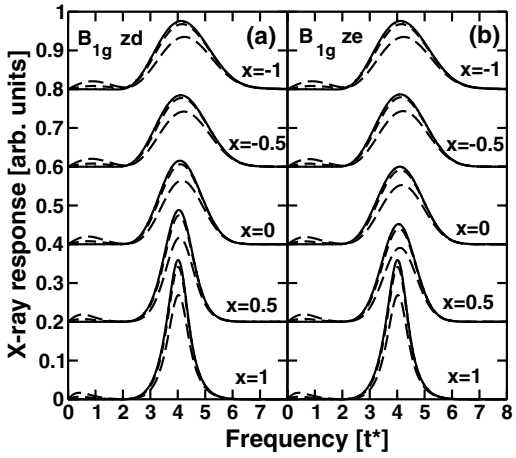


FIG. 3. Inelastic x-ray scattering response in the $B_{1g}$ channel along (a) the Brillouin zone diagonal and (b) along the zone edge for the half-filled Falicov-Kimball model on a hypercubic lattice. The solid, dotted, short-dashed, and long-dashed curves correspond to temperatures $T = 0.1$, 0.25 (partially obscured by the 0.1 line), 0.5, 1.0, respectively.

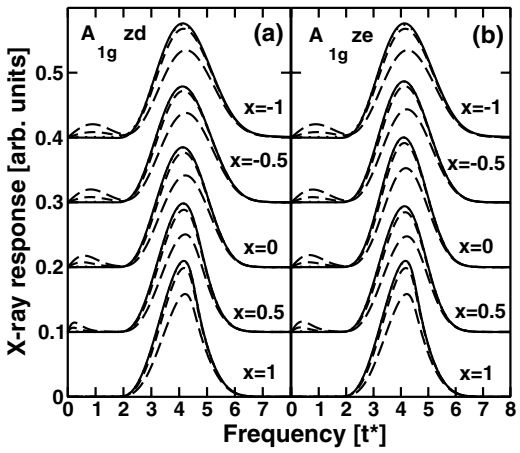


FIG. 4. Inelastic x-ray scattering response in the $A_{1g}$ channel along (a) the Brillouin zone diagonal and (b) along the zone edge for the half-filled Falicov-Kimball model on a hypercubic lattice. The solid, dotted, short-dashed, and long-dashed curves correspond to temperatures $T = 0.1$, 0.25 (partially obscured by the 0.1 line), 0.5, 1.0, respectively.

relatively dispersionless due to the local nature of the correlations. In contrast, the low-energy feature is a consequence of thermally generated double occupancies which open a low-energy band (up to energies $\sim t^*$) able to scatter x rays. For decreasing temperature, the low-energy intensity disappears and only scattering across the Mott gap remains.

The charge-transfer peak is sharp near the BZ center ($X = 1$), but broadens for momentum transfers approaching the BZ corner $X = -1$, more so for the $B_{1g}$ channel than for $A_{1g}$. In fact, the $A_{1g}$ and $B_{1g}$ responses are identical at the $(\pi, \pi, \ldots, \pi)$ point $X = -1$ due to the local approximation. Any variation in the signal at the zone corner in different symmetry channels is due to nonlocal many-body correlations.

An important difference is that the $A_{1g}$ results have no low-energy spectral weight for $\mathbf{q} = 0$, corresponding to inelastic Raman scattering [9]. The vertex corrections remove all remnants of the low-energy response here, but it enters for any finite value of $\mathbf{q}$. For an unpolarized (partially polarized) measurement, the x-ray response is a (weighted) superposition of the $B_{1g}$ and $A_{1g}$ spectra.

We plot the behavior of the peak position and peak width (full-width at half maximum) for both the low-energy peak and the charge-transfer peak for both channels in Fig. 5. One can see that the low-energy peak has a width larger than its energy for both channels and for the $A_{1g}$ channel follows the behavior of the corresponding $B_{1g}$ feature away from the zone center. The charge-transfer peak is well defined for both channels. The only dispersive feature of the charge-transfer peak is the width of the $B_{1g}$ peak.

Referring back to the experimental data shown in Fig. 1, it is tempting to associate the relatively dispersionless high-energy peak with an excitation across a charge-transfer gap and the broad low-energy peak with the dispersive feature generated from double occupancies. However, the experimental data are not yet complete as the polarization and temperature dependence have not been measured. Our theory predicts that the low-energy feature decreases in intensity as temperature is lowered. Moreover, a polarization-dependent measurement could perhaps deconvolve the high-energy peak into two separate peaks of $A_{1g}$ and $B_{1g}$ symmetry, and would also be able to separate different behavior of the low-energy peak near the zone center. Thus we believe it is interesting to examine inelastic x-ray scattering at different temperatures and with polarizers for the incident and scattered light. We believe that a number of new and interesting features of charge excitations in correlated systems are likely to emerge if this can be accomplished.

In summary, we have constructed a formally exact theory for nonresonant x-ray scattering in correlated insulators to determine the pathways for electron relaxation in strongly correlated systems. We find that a high-energy charge-transfer peak and a low-energy peak both broaden and disperse through the Brillouin zone similar to what is seen in experiments in $Ca_2CuO_2Cl_2$. In general, the temperature and polarization dependence of the spectrum would assist in an interpretation of observed peaks in the x-ray spectrum of correlated insulators.

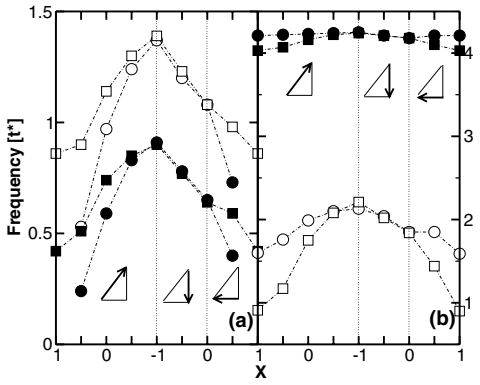


FIG. 5. Plots of the low-energy (panel a) and charge-transfer (panel b) peak positions (solid symbols) and broadening (full width at half maximum, open symbols) for $T = t^*$ determined from Figs. 3 and 4 for $A_{1g}$, $B_{1g}$ (circles, squares), respectively.

We would like to thank M. Z. Hasan and Z.-X. Shen for sharing their experimental data with us and thank them and J. P. Hill and M.V. Klein for valuable discussions. J. K. F. acknowledges support from the NSF under Grants No. DMR-9973225 and No. DMR-0210717. T. P. D. acknowledges support by NSERC and PREA.

[1] For a review, see A. Kotani and S. Shin, Rev. Mod. Phys. **73**, 203 (2001).
[2] P. Abbamonte *et al.*, Phys. Rev. Lett. **83**, 860 (1999); Y. K. Kim *et al.*, Phys. Rev. Lett. **89**, 177003 (2002).
[3] M. Z. Hasan *et al.*, Science **288**, 1811 (2000); M. Z. Hasan *et al.*, Physica (Amsterdam) **364C–365C**, 618 (2001).
[4] G. P. Zhang *et al.*, Phys. Rev. Lett. **88**, 077401 (2002).
[5] K. Hämäläinen *et al.*, Phys. Rev. B **61**, 1836 (2000); J. P. Hill *et al.*, Phys. Rev. Lett. **80**, 4967 (1998).
[6] M. Z. Hasan *et al.*, Phys. Rev. Lett. **88**, 177403 (2002); (private communication).
[7] K. Tsutsui, T. Tohyama, and S. Maekawa, Phys. Rev. B **61**, 7180 (2000); K. Okada and A. Kotani, Phys. Rev. B **65**, 144530 (2002).
[8] T. P. Devereaux and A. P. Kampf, Int. J. Mod. Phys. B **11**, 2093 (1997).
[9] J. K. Freericks and T. P. Devereaux, Condens. Matter Phys. **4**, 149 (2001); Phys. Rev. B **64**, 125110 (2001).
[10] J. K. Freericks, T. P. Devereaux, and R. Bulla, Phys. Rev. B **64**, 233114 (2001).
[11] L. M. Falicov and J. C. Kimball, Phys. Rev. Lett. **22**, 997 (1969).
[12] A. M. Shvaika, Physica (Amsterdam) **341C–348C**, 177 (2000); J. K. Freericks and P. Miller, Phys. Rev. B **62**, 10022 (2000); A. M. Shvaika, J. Phys. Stud. **5**, 349 (2002).
[13] A. Khurana, Phys. Rev. Lett. **64**, 1990 (1990).
[14] U. Brandt and C. Mielsch, Z. Phys. B **75**, 365 (1989); V. Zlatić *et al.*, Philos. Mag. B **81**, 1443 (2001).